Corrigendum to The Cryosphere, 15, 2873–2888, 2021
https://doi.org/10.5194/tc-15-2873-2021-corrigendum

The Cryosphere
Open Access
EGU

Corrigendum to "Non-normal flow rules affect fracture angles in sea ice viscous–plastic rheologies" published in The Cryosphere, 15, 2873–2888, 2021

Damien Ringeisen[1,2], **L. Bruno Tremblay**[3], **and Martin Losch**[1]

[1]Alfred-Wegener-Institut, Helmholtz-Zentrum für Polar- und Meeresforschung, Bremerhaven, Germany
[2]MARUM – Center for Marine Environmental Sciences, Leobener Str. 8, 28359, Bremen, Germany
[3]Department of Atmospheric and Oceanic Sciences, McGill University, Montréal, Canada

Correspondence: Damien Ringeisen (damien.ringeisen@awi.de)

Published: 16 August 2023

Abstract. The deformation in a viscous–plastic sea ice model is defined by a flow rule that is normal to the plastic potential in stress space. When the plastic potential is identical to the yield curve, the flow rule is termed "normal" and is normal to both the plastic potential and the yield curve. When the plastic potential and yield curve are not identical, the flow rule is termed "non-normal" and the deformation (still normal to the plastic potential) is no longer normal to the yield curve. In Ringeisen et al. (2021), states of stress on the elliptical plastic potential and yield curve were assumed to have the same mean normal stress (or first stress invariant); i.e., the stress states on the plastic potential were translated in the vertical along the second stress invariant axis (maximum shear stress). In fact this translation should take place along a line that passes through the center of the elliptical yield curve (or plastic potential). It follows that the simulated fracture angle in (numerical) uni-axial loading experiments follows Arthur's angle, as opposed to Roscoe's angle, as stated in Ringeisen et al. (2021). However, the implementation of the rheology and the simulated angles do not change; only their interpretation is different.

The paper initially submitted for publication contained some analysis of results that has since been interpreted differently. An updated interpretation is given in the following.

1 Introduction

Ringeisen et al. (2021) introduced an elliptical plastic potential (with a different ellipse aspect ratio) in the most common viscous–plastic sea ice model with an elliptical yield curve in order to study the impact of a non-normal (or non-associated) flow rule on the failure angles.

2 Rheological formulation

The elliptical yield curve and plastic potentials can be written as

$$\sigma_{\mathrm{II}} = \frac{1}{e_X}\sqrt{P^2 k_t - \sigma_{\mathrm{I}}^2 - \sigma_{\mathrm{I}} P(1-k_t))}, \tag{1}$$

where $X = F$ for the yield curve and $X = G$ for the plastic potential. The bulk ζ and shear η viscosities can be written as

$$\zeta = \frac{P(1+k_t)}{2\Delta}, \tag{2}$$

$$\eta = \frac{P(1+k_t)}{2e_G^2\Delta}, \tag{3}$$

where

$$\Delta = \sqrt{\dot{\epsilon}_{\mathrm{I}}^2 + \frac{e_F^2}{e_G^4}\dot{\epsilon}_{\mathrm{II}}}, \tag{4}$$

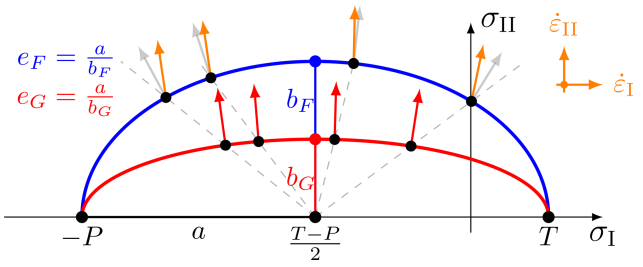

Figure 1. Figure 2 of Ringeisen et al. (2021), corrected. Elliptical yield curve with a non-normal flow rule, a yield curve ellipse aspect ratio $e_F = 2$ (blue), and a plastic potential ellipse aspect ratio $e_G = 4$ (red). The gray and orange arrows show the normal and non-normal flow rules, respectively.

$\dot{\epsilon}_I$ is the divergence, $\dot{\epsilon}_{II}$ is the maximum shear strain rate, and P is the thickness-dependent (h) and concentration-dependent (A) ice strength. The constitutive equations for the stress can be written in invariant space as

$$\sigma_I = \zeta \dot{\epsilon}_I - \frac{1-k_t}{2} P, \tag{5}$$

$$\sigma_{II} = \eta \dot{\epsilon}_{II}. \tag{6}$$

This is the exact same implementation as in Ringeisen et al. (2021), and it does not change in the following.

3 Non-normal flow rule

We previously stated that "The flow rule for a given stress on the yield curve is normal to the plastic potential for the same σ_I" (also called first stress invariant). While we found this to be true for other yield curves, such as the modified Coulombic yield curve (Hibler and Schulson, 2000; Ringeisen et al., 2019), this is not the case for the elliptical yield curve with an elliptical plastic potential of different ellipse aspect ratio. Instead, the orientation of the flow rule for a given stress point on the yield curve is normal to the plastic potential at the intersection with a line passing by the center of the ellipse and the given stress point on the yield curve (Fig. 1).

Mathematically, the orientation of the flow rule, or dilatancy, can be expressed as $\delta = \arctan\left(\frac{\dot{\epsilon}_I}{\dot{\epsilon}_{II}}\right)$ (Tremblay and Mysak, 1997). Using Eqs. (5) and (6) we can express δ as function of σ_I as

$$\begin{aligned}\delta &= \arctan\left(\frac{2\eta(\sigma_I + \frac{1-k_t}{2}P)}{\zeta \sigma_{II}}\right) \\ &= \arctan\left(\frac{e_F}{e_G^2} \frac{\sigma_I + \frac{1-k_t}{2}P}{\sqrt{k_t P^2 - \sigma_I(\sigma_I + P(1-k_t))}}\right).\end{aligned} \tag{7}$$

The flow rule now depends on both e_F and e_G, as opposed to e_G alone (Eq. 27; Ringeisen et al., 2021):

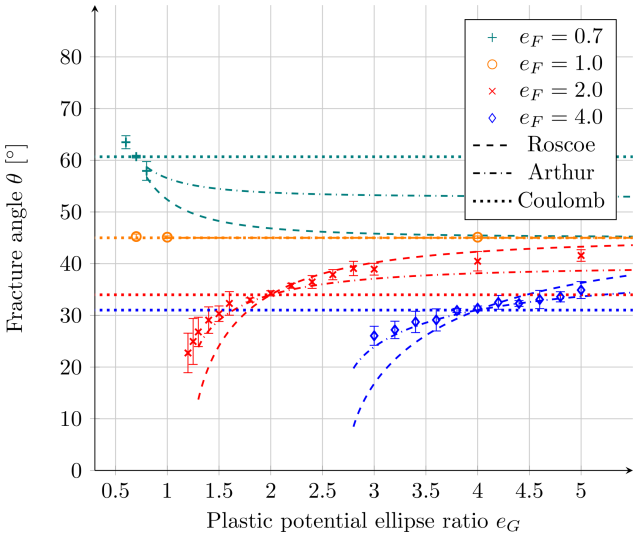

Figure 2. Figure 7a of Ringeisen et al. (2021), corrected. Note that only the Roscoe angles changed and the Arthur angles were added; everything else remains the same. Fracture angles as a function of the plastic potential ellipse ratio e_G for different yield curve ellipse ratios ($e_F = 0.7$, 1.0, 2.0, and 4.0). The markers with ranges are the mean and 2 standard deviations of the fracture angles. The dashed lines show the Roscoe angle (Eq. 9), and the dash-dotted lines show the Arthur angles (Eq. 11). The dotted lines mark the Coulomb angles as a function of e_F, which are constant with respect to e_G. Colors indicate the value of e_F for lines and markers. For the Arthur angles, the R^2 values between theory and modeled angles for $e_F = 0.7$, 2.0, and 4.0 are 0.94, 0.83, and 0.88.

$$\begin{aligned}\delta_G &= \frac{\partial \sigma_{II,G}}{\partial \sigma_I} \\ &= \arctan\left(\frac{1}{e_G} \frac{\sigma_I + \frac{1-k_t}{2}P}{\sqrt{k_t P^2 - \sigma_I(\sigma_I + P(1-k_t))}}\right).\end{aligned} \tag{8}$$

4 Relationship to failure angles

For uni-axial compression ($\sigma_{II} = -\sigma_I$ or $\sigma_1 = 0$) and $k_t = 0$, the Roscoe angles for the elliptical yield curve with ellipse aspect ratios e_F and e_G can be written as (using Eq. 7)

$$\theta_R = \frac{1}{2} \arccos\left(\frac{1}{2e_G^2}\left(e_F^2 - 1\right)\right). \tag{9}$$

This reduces to the normal flow rule case ($e_F = e_G$; Ringeisen et al., 2021):

$$\theta_C = \frac{1}{2} \arccos\left(\frac{1}{2}\left(1 - \frac{1}{e_F^2}\right)\right). \tag{10}$$

The Arthur angles θ_A are given, using Eqs. (9) and (10), by

$$\theta_A = \frac{1}{2}(\theta_C + \theta_R). \tag{11}$$

Unlike what we previously stated, the failure angles with the elliptical yield curve with an elliptical plastic potential follow the predictions of the Arthur angles (Fig. 2). The RMSEs between the modeled angles and the Arthur angles are 0.57, 0.16, 2.1, and 0.918° for $e_F = 0.7$, 1.0, 2.0, and 4.0, respectively. The simulated angles (the markers with error bars in Fig. 2) did not change; only the predicted Roscoe angles changed.

5 Conclusions

The failure angles with an elliptical yield curve and non-normal flow rule instead follow the Arthur angles. The use of a non-normal flow rule still reduces the magnitude of the failure angles.

Author contributions. DR and BT found the discrepancy in the flow rule behavior. DR derived the new equations, remade the figures, and wrote the first manuscript draft. All authors edited the manuscript.

Acknowledgements. This project contributes to the Natural Sciences and Engineering Research Council Discovery program and the Grants and Contributions from Environment and Climate Change Canada awarded to L. Bruno Tremblay.

References

Hibler, W. D. and Schulson, E. M.: On modeling the anisotropic failure and flow of flawed sea ice, J. Geophys. Res.-Oceans, 105, 17105–17120, https://doi.org/10.1029/2000JC900045, 2000.

Ringeisen, D., Losch, M., Tremblay, L. B., and Hutter, N.: Simulating intersection angles between conjugate faults in sea ice with different viscous–plastic rheologies, The Cryosphere, 13, 1167–1186, https://doi.org/10.5194/tc-13-1167-2019, 2019.

Ringeisen, D., Tremblay, L. B., and Losch, M.: Non-normal flow rules affect fracture angles in sea ice viscous–plastic rheologies, The Cryosphere, 15, 2873–2888, https://doi.org/10.5194/tc-15-2873-2021, 2021.

Tremblay, L.-B. and Mysak, L. A.: Modeling Sea Ice as a Granular Material, Including the Dilatancy Effect, J. Phys. Oceanogr., 27, 2342–2360, https://doi.org/10.1175/1520-0485(1997)027<2342:MSIAAG>2.0.CO;2, 1997.